

We are IntechOpen, the world's leading publisher of Open Access books Built by scientists, for scientists

7,000

Open access books available

186,000

International authors and editors

200M

Downloads

Our authors are among the

154

Countries delivered to

TOP 1%

most cited scientists

12.2%

Contributors from top 500 universities



WEB OF SCIENCE™

Selection of our books indexed in the Book Citation Index
in Web of Science™ Core Collection (BKCI)

Interested in publishing with us?
Contact book.department@intechopen.com

Numbers displayed above are based on latest data collected.
For more information visit www.intechopen.com



Chapter

A Review on Vacuum-Powered Fluidic Actuators in Soft Robotics

Seonggun Joe, Federico Bernabei and Lucia Beccai

Abstract

In the past few years, vacuum-powered soft actuators have shown strong potential due to their promising mechanical performance (i.e., fail-safe, fast response, compactness, robustness, jamming, etc.). Indeed, they have been widely exploited in soft robots, for example, grippers and manipulators, wearable devices, locomotion robots, etc. In contrast to inflatable fluidic actuators, the properties of the materials with which they are built have a stronger influence on the kinematic trajectory. For this reason, understanding, both, the geometry and morphology of the core structure, and the material characteristics, is crucial to achieving the desired kinetics and kinematics. In this work, an overview of vacuum-powered soft fluidic actuators is provided, by classifying them as based on morphological design, origami architecture, and structural instability. A variety of constitutive materials and design principles are described and discussed. Strategies for designing vacuum-powered actuators are outlined from a mechanical perspective. Then the main materials and fabrication processes are described, and the most promising approaches are highlighted. Finally, the open challenges for enabling highly deformable and strong soft vacuum-powered actuation are discussed.

Keywords: vacuum-powered actuation, pneumatic artificial muscle, linear actuation, origami structural instability, morphological design, buckling, hyperelastic materials, 3D printing, soft robotics

1. Introduction

In the recent past, Pneumatic Artificial Muscles (PAMs) have assumed a key role in the implementation of movement in soft robots. The strong research attention is due to their interesting mechanical characteristics for soft actuation (i.e., robustness, high pulling force, high-power to mass ratio, and high energy efficiency), compared to other mechanisms exploiting different actuation sources (i.e., electric motor or tendon driven [1, 2], piezoelectric actuators [3], dielectric elastomer actuators [4, 5], shape memory alloys [6, 7] or polymers [8], and ionic polymer-metal composite actuators [9], etc.). Many researchers and engineers have explored quite a few design principles for PAMs, and a wide range of robotic applications was introduced (i.e., industrial robots [10, 11], wearable [12–14], or medical devices [15–17], etc.) where some of the challenges that rigid-bodied robots cannot overcome were addressed [18–21].

From the material point of view, PAMs are generally built from soft materials that can undergo large deformation under external forces. Softness may result from their intrinsic characteristics (i.e., chemistry) or because of a specific design of their structure [22], or both.

In the design phase, the mechanical performance of PAMs (i.e., deformation ratio and blocking force) can be tuned by optimizing some geometrical parameters to achieve specific morphologies. In particular, a tradeoff between deformability and stiffness should be met, depending on the desired mechanical performances. In the literature, different design principles have been used. As most of such designs show, radial strain is an important parameter given its main influence on the linear deformation ratio of the soft actuator.

Most soft pneumatic actuators operating with positive pressure (also called inflatable fluidic actuators) involve—(i) a section of the actuator that expands with pressure; or (ii) strain limiting components that guide the elastic expansion in the desired direction [23].

In the former case, topological and/or morphological approaches are undertaken to produce radial expansion/contraction by employing specific geometries, such as zig-zag patterned pleats or convolutions. For instance, the Peano fluidic actuator consists of a set of tubes arranged side-by-side [24]. At null pressure (atmospheric pressure), the actuator remains completely flat. Once positive pressure is applied, each cylindrical tube is inflated, leading to a vertical contraction. Another example is to exploit a bellow that can reduce radial strain, and enlarge longitudinal strain. This design principle is quite useful since biaxial deformability (contraction and elongation) is enabled upon positive pressure and vacuum [25, 26]. In the latter case (ii) multi-material-based approaches were addressed, such as in McKibben actuators or pleated PAMs (PPAMs). A McKibben actuator generally consists of a cylindrical flexible rubber and/or silicone bladder, sheathed with an inextensible fiber network intersected at a certain angle [27, 28]. Different kinematic trajectories are enabled according to the intersection angle (e.g., extension at the intersection angle of more than 54.7 deg., otherwise contraction) [29, 30]. On the other hand, a PPAM generally consists of a membrane having many pleats, with high tensile stiffness (i.e., woven polyester cloth or Kevlar fabric) [31, 32]. This allows the actuators to contract with dramatic increases in diameter when positive pressure is applied. The pleats are arranged along the longitudinal direction, and as the skin begins to swell, the overall structure undergoes a radial shortening and expansion [33].

As mentioned above, desired mechanical performance for inflatable fluidic actuators can be achieved by adopting proper design principles. Nevertheless, the mechanisms exploiting volumetric expansion are commonly vulnerable, depending on material failures (i.e., delamination, fracture), resulting in degradation of the actuator, and poor reliability. Moreover, given the needed volumetric expansion and omnidirectional deformation, they are more likely to be applied where large spaces are available [23]. Vacuum-powered pneumatic artificial muscles (or V-PAMs) represent a promising opportunity in soft actuation and solve some of the issues encountered by inflatable fluidic actuators. They rely on decreasing the volume with vacuum and, generally, they do not expand radially during movement. Rather, they can perform linear movements with a relatively low input vacuum pressure (within few hundred kPa) and avoid a stress concentration that could possibly incur along the overall structure at both local and global levels [34, 35]. These characteristics are pursued to achieve high reliability, and ensure a high bandwidth, allowing to saturate at the desired state with a fast response.

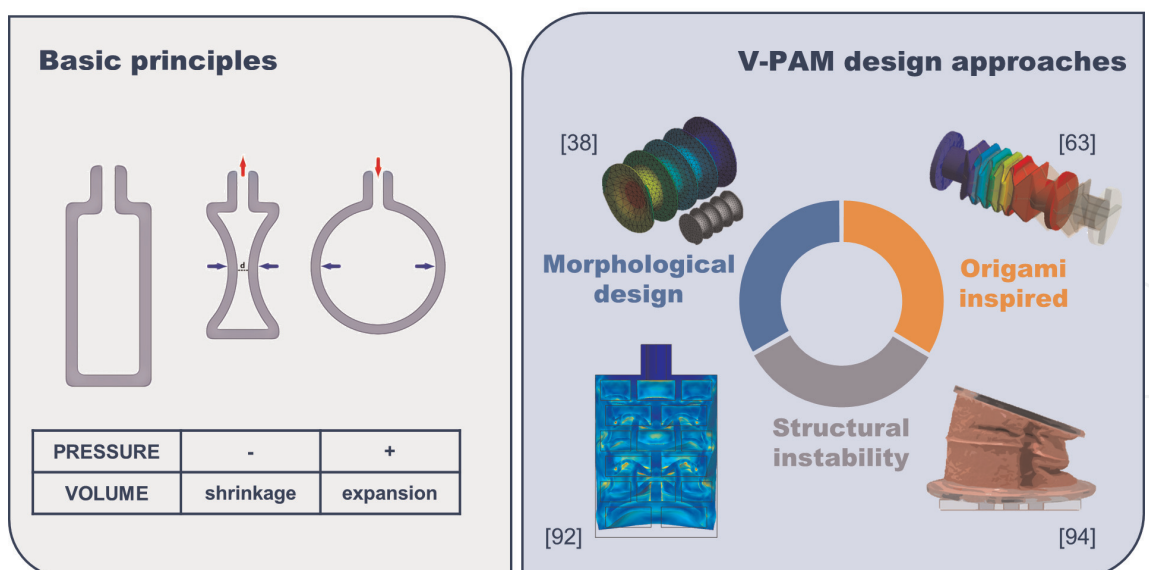


Figure 1. Left, basic operating principles of pneumatic artificial muscles (PAMs). Right, a classification of vacuum-powered PAMs (V-PAMs) based on the different design approaches: morphological design [38]; origami inspired [63]; structural instability shown in FEM model of the buckling actuator [92], and reproduced with permission [94].

As with inflatable fluidic actuators, the constituting materials strongly influence performance, particularly the deformation ratio. Indeed, due to the incompressibility of the materials, the ratio of bulk modulus (K) to shear modulus (G) is extremely large or becomes almost infinite in case Poisson's ratio is close to 0.5 [36]. Thus, only a slight shortening is achievable until internal walls contact, and collapse, and linear deformation hardly occurs, as shown in **Figure 1**. Moreover, the overall deformations generally include undesired kinematic trajectories (i.e., torsion or bending) due to structural instability (i.e., column squirm and/or buckling). For these reasons, V-PAMs need to be rigorously designed by taking into account geometry and/or morphology, structural stability for imposed deformation and/or load, etc.

Various design principles can be found for V-PAMs in the literature, however (to the authors' knowledge), there are still no comprehensive articles on such an emerging topic, including design, fabrication, and materials. In this work, an overview of the developments of vacuum-powered actuators is provided and they are classified as based on morphological design, origami architecture, and structural instability. The fabrication protocols and soft materials involved are addressed, and their advantages and limitations are discussed and compared.

2. Design

2.1 Morphological design

Soft pneumatic actuators can benefit from designs having zigzag patterns since they enable shear deformation, by enlarging deformations while avoiding structural instability. Typical designs consist of multiple convolutions or corrugations in series along the vertical or horizontal direction of the actuator. In this section, an overview of different types of morphological designs, including actuators with convoluted (or corrugated) skin and pleated skin, is provided by highlighting their pros and cons.

2.1.1 Convoluted skin

Convolution and/or corrugation in skin design includes a crumpled thin membrane. A bellow represents a unique structure made of multiple convolutions periodically arranged along the vertical direction of the structure, as shown in **Figure 2a**. In principle, its mechanical performance can be determined by geometrical parameters (i.e., number of convolutions, mean diameter, total length, etc.). The deformation can be defined as either positive or negative when subjected to extension or compression. In accordance with EJMA¹ standard, the axial stiffness per convolution can be written as [41, 42]:

$$f_{iu} = 1.7 \frac{D_m E_b t_p^3 n}{w^3 c_f} \quad (1)$$

where C_f is a non-dimensional parameter, and D_m , E_b , t_p , n , and w , indicate geometric parameters of the bellow skin (see **Figure 2a–c** and nomenclatures summarized in **Table A1** in the Appendix). Alternatively, Wang et al. deduced the axial deformation by means of Castiglano's theorem, and derived the axial stiffness [25], as follows:

$$f_{iu} = \frac{\pi E_b t_p^3}{3N(1 - \mu^2)d^2 \left[\ln \frac{D}{d} - \left(\frac{D}{d} - 1 \right) + \frac{\left(\frac{D}{d} - 1 \right)^2}{2} \right]} \quad (2)$$

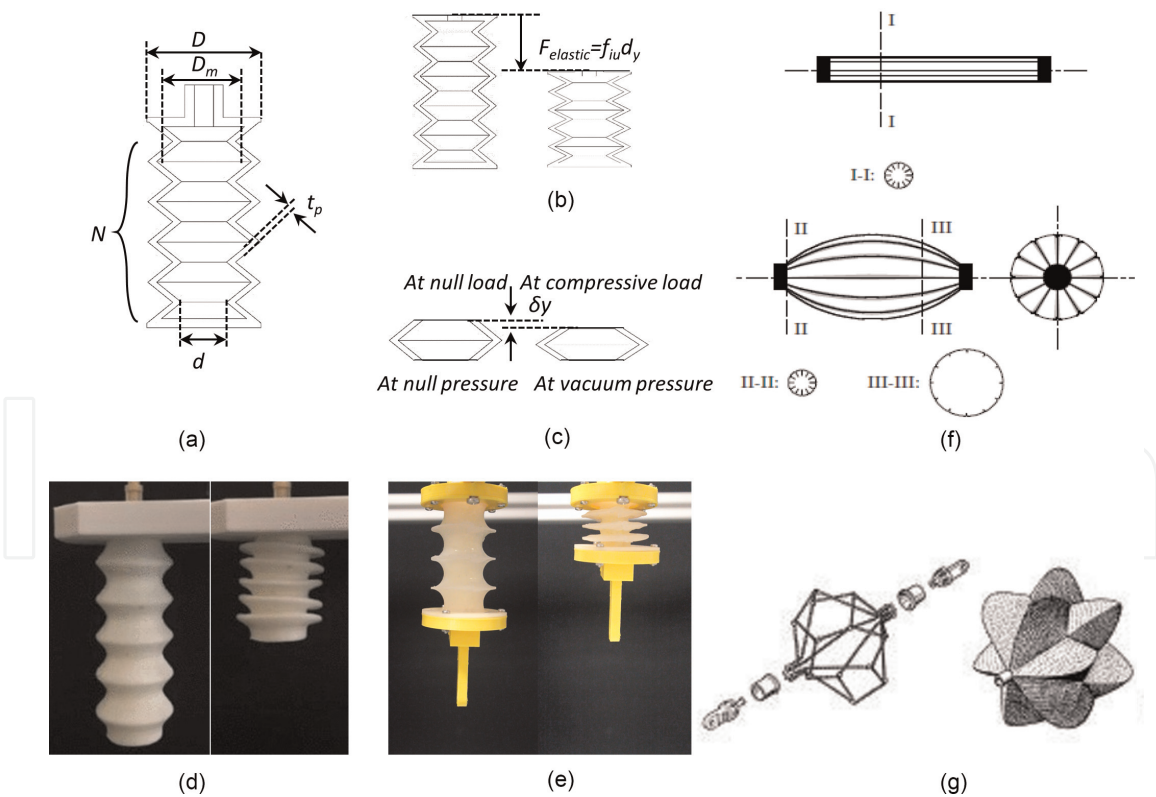


Figure 2.

V-PAMs with morphological design. (a–c) schematic diagrams that show design parameters for a bellow actuator skin. (d) the 3D-printed linear soft vacuum actuator (L-SOVA). Reproduced with permission [37]. (e) the Ultralight Hybrid PAM (UH-PAM) capable of 52% contraction [38]. (f) the Pleated Pneumatic Artificial Muscle (P-PAM) [39]. (g) the Robotic Muscle Actuator (ROMAC) [40].

¹ EJMA: Expansion Joint Manufacturers Association <https://www.ejma.org/>

Given Hooke's law ($F_{elastic} = f_{iu}d_y$), the axial stiffness along the y-axis, and the imposed deformation (d_y), identify the elastic force of the bellow structure ($F_{elastic}$). The blocking force of the actuator can be approximated by using a quasi-static analytical model [43, 44]. The work produced by the distributed pressure acting on the inner wall of the skin can be expressed [38] by

$$-F_t \cdot \delta y = P \cdot dv \quad (3)$$

where P and dv are the gauge pressure and the change in the actuator's volume, respectively. Then, the exerted force (also corresponding to the blocking force) at the free end of the actuator can be represented by the derivative of the cross section [45]. The ratio of the outer diameter to the inner diameter (D/d) can be represented as a function of displacement. To the authors' knowledge, it is not possible to approximate the change in volume of actuator explicitly, while it can be obtained by taking into account specific assumptions (e.g., exploiting either geometrical constraints or the material incompressibility) [38]. Indeed, given that the bellows are made of soft or composite materials, they can achieve a linear displacement [46], and it should be highlighted that modeling of the bellow structure is mainly due to the variation in the overall length, rather than radial strain.

Moreover, from Eqs. (1)–(3), it is worth mentioning that the axial stiffness of the bellow is strongly influenced by the skin thickness (t_p) (with cubic order). Also, the higher the number of convolutions, the more compliant the actuator structure is likely to be (i.e., weak stiffness). However, the skin thickness could limit deformability of the bellow at the collapsed state. Thus, both the number of convolutions and skin thickness are important design parameters, determining the axial stiffness and deformability of the overall structure.

Based on such theoretical background, several examples can be found in the literature. Digumarti et al. presented a Hyper-Elastic Bellow (HEB) actuator capable of a euglenoid motion, where both axial and radial strains are enlarged [26]. The bellow, having a half angle of 38.66° with a total length of 50 mm and an outer diameter of 45 mm, was fabricated by using a soft elastomer (Dragon Skin™ 10 SLOW, Smooth-On). The HEB was capable of 40% contraction upon a small vacuum pressure of 8 kPa. More recently, by exploiting additive manufacturing, Tawk et al. presented a 3D-printed Linear Soft Vacuum Actuator (L-SOVA), capable of 51% contraction with a payload of 27.66 N. Another example is to exploit the integration of rigid parts (rings), periodically spaced along the actuator length. This way, Felt et al. showed that a bellow type PAM, made of a tubular thin membrane, can lift a high payload of 21.35 N at -5.52 kPa [47]. Such investigation on V-PAMs has demonstrated that this kind of actuation can enable a high contraction ratio and blocking force, opening the way to new PAM concepts. In refs. [38, 48], our group exploited rigid rings to improve axial stiffness and combined them with open-cell foam modules to build an Ultralight Hybrid PAM (UH-PAM) made of open-cell foam and elastomeric bellow skin (see **Figure 2e**). In this study, we investigated an optimal geometry of the skin and emphasized that even with a light weight of 20 g promising mechanical characteristics can be achieved. Due to the open-cell foam and rigid rings interfaced at each convolution, the axial stiffness of UH-PAM was enhanced, resulting in a high payload of 3 kgf and a high contraction ratio of 52%.

Furthermore, a bellow textile muscle (similar to the Peano fluidic muscle), made of fabric and multiple round discs along its edges and center, was developed to enlarge the deformation ratio [49]. Due to such inflatable and flexible material, the bellow's

textile muscle can be displaced to extremely flat (i.e., high contraction ratio of 89%) with a high payload of 32 N at -5 kPa. Recently, Yang et al. extended this work and presented a high-displacement PAM, converting the horizontal motion of the bellow actuator to a vertical motion, based on the contraction when subjected to positive air pressure [45]. Given that the contraction ratio of the bellow is strongly influenced by its thickness, exploiting textile for the skin enables to deform it to a completely flat configuration, upon vacuum pressure. On the other hand, the thin-walled structure could suffer from a lack of axial stiffness. Thus, the bellow structure does not sustain its own weight, which implies that the actuator cannot be set along the horizontal direction (e.g., beam orientation), and it should be placed along the gravity direction. Hence, for vacuum-powered bellow actuators, both enhancing the axial stiffness, and reducing the total weight remain open challenges.

2.1.2 Pleated skin

A typical pleated airtight membrane creates chambers enabling a linear motion upon vacuum pressure, due to a similar morphological feature of the Robotic Muscle Actuator (also called ROMAC muscle) [40], as shown in **Figure 2f** and **g**. While to the authors' knowledge no vacuum-powered PAMs exploiting this principle can be found in the literature up to date, presumably mechanical benefits would be significant rather than contractile actuators operated by only positive pressure. Indeed, the created folds distributed along the circumference of the structure allow biaxial deformations. They can be depressurized until the internal walls touch. In principle, the compressibility of the air chamber enables radial contraction, resulting in elongation of the structure upon the vacuum pressure. On the other hand, the air chambers enable the overall structure to exhibit extension upon positive pressure due to significant radial expansion. Such biaxial deformability, mainly due to the deformation in the radial direction, could play a key role in keeping the volume constant during inflation/deflation (i.e., the muscular hydrostat principle [50]), and in enlarging a linear displacement, rather than uniaxial deformation that many PAMs have accomplished so far. Moreover, the tension force that the pleated PAM can produce is adjustable. From a theoretical point of view, the tension force (F_t) generated by the imposed positive pressure (P) is strongly influenced by the number of pleats (k) [51], as follows:

$$F_t = P \frac{k}{2\pi} \sin\left(\frac{2\pi}{k}\right) l_0^2 f\left(\epsilon, \frac{l_0}{R}\right) \quad (4)$$

where l_0 and R indicate the initial length and radius, respectively. An example of a device accomplishing this behavior is a cylindrical structure having coupled and parallel fluidic channels arranged along its circumference [20]. Due to the adjustability of radial extension and contraction, Hao et al. developed a fingerless soft gripper capable of multiple grasping modes. In order to have large deformation, such structures should have optimized pleated patterns, and they should be fabricated with the hyperelastic materials.

2.2 Origami-inspired design

Origami is a unique technique inspired by Japanese paper folding, which can be created by folding thin sheets along the predefined creases [52–54]. There are three identical crease patterns in the origami, which are the Yoshimura pattern, Miura-ori

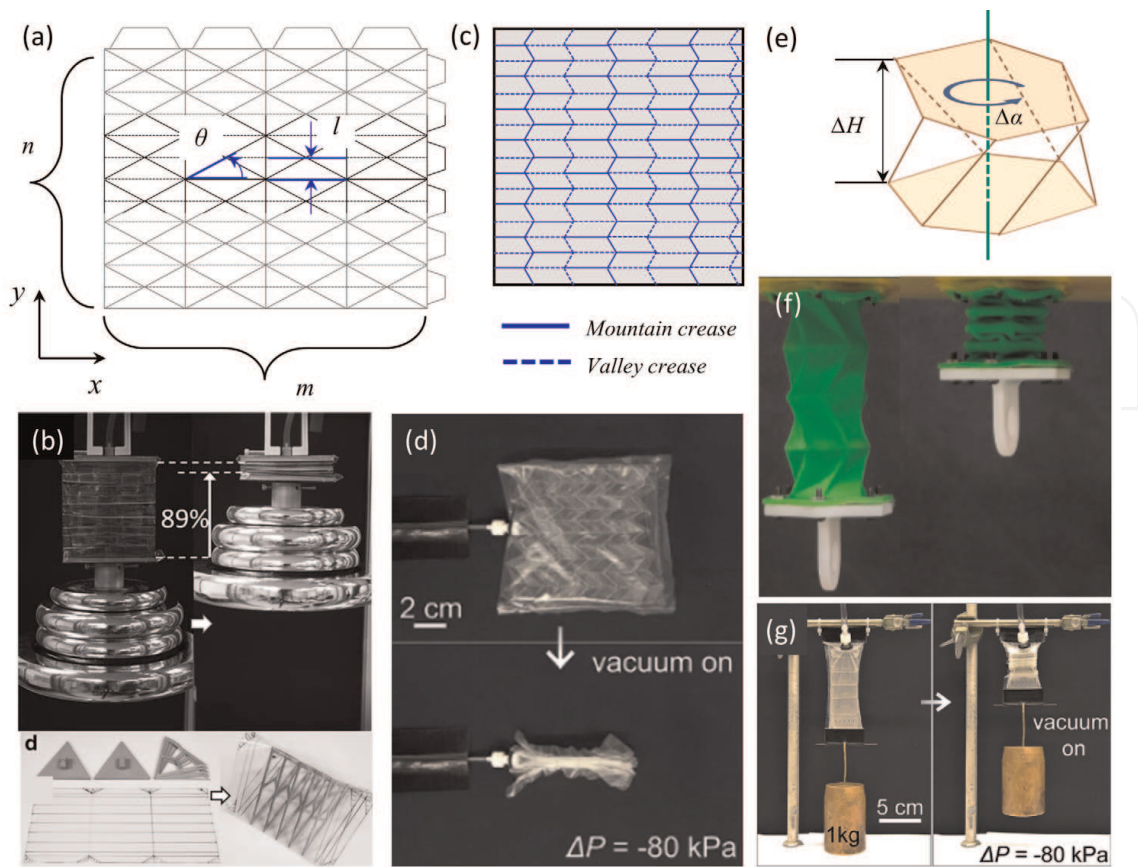


Figure 3. Origami-inspired design approaches. (a) 2D crease pattern of the 4 x 6 Yoshimura-Ori (DoFs = 26, $m = 4$, $n = 6$). (b) an equilateral triangular shaped Origami-based vacuum PAM (OV-PAM) capable of contraction ratio up to 90% and blocking force up to 400 N. Reproduced with permission [43]. (c) a 2D crease pattern of the Miura-Ori (solid and dashed lines indicate mountain and valley creases, respectively). (d) the Miura-Ori based surface skeleton capable of a 92% contraction [57]. (e) a geometry of the crease pattern of the Kresling pattern. (f) a 3D printed origami V-PAM capable of purely axial movement due to the even number of reversed diagonal creases. Reproduced with permission [58]. (g) a lightweight origami skeleton-based actuator (2.6 g) capable of a payload of 3 kgf [57].

pattern, and Kresling (diagonal) pattern [55]. Depending on delivering motion, active or passive origami can be defined – the active origami exhibits movements through the embedded mechanism and/or structure itself. However, passive origami exhibits the motions derived from other actuation sources. Moreover, either supporting motions (i.e., structural stiffness enhancement) or achieving programmable motions can be achieved [56].

As regards the active origami, the deformability is commonly given by a function of a geometrical length (l) in the origami unit and the intersection angle of two facets (θ) (See **Figure 3a**) [59]. From the kinematics point of view, the number of creases is crucial to determine the overall structure's compliance (e.g., for the Yoshimura pattern, $\text{DOF} = 9 + 4 \cdot (m-1) + (n-1)$, with m and n indicating the number of basic creases in x and y direction, respectively [60]). The output force can be represented [43] by

$$F = -PA_e \quad (5)$$

where A_e indicates an effective area (i.e., cross section) of the structure. Note that in the case the origami structure is made of polymers, an inflated state could be approximated as a circle due to its omnidirectional deformation. On the other hand,

the deflated state needs to be rigorously modeled because the deformation occurs along the crease originated upon vacuum pressure. Therefore, to precisely predict the kinematics actuator, the effective area (i.e., cross section) should be taken into account.

In the following, an overview of origami-inspired pneumatic actuators made of different crease patterns is provided, and their design principles allowing for linear motions upon vacuum pressure are introduced.

2.2.1 Yoshimura patterned unit cell

The Yoshimura pattern, enabling foldable and deployable 3D structure, was introduced in 1955 by a Japanese scientist who first observed a buckling at thin-walled cylinders upon axial compression [53]. The Yoshimura pattern consists of identical isosceles triangles symmetrically connected in each row [56]. This way, it generates a purely translational motion element with high axial stiffness. Due to these characteristics, the Yoshimura pattern can be exploited as, both, a passive origami to reinforce movements [61], and an active origami capable of axial movement [62].

Based on the Yoshimura patterns, Martienz et al. presented novel design principles for actuators to respond to pressurization with a wide range of motions (i.e., bending, extension, contraction, twisting, etc.) [62]. A bellow morphology made of 10 creases enabled high deformability, up to 361% at 17 kPa, and the lifting of high payloads, that is, 1 kgf being 120 times its own weight (8.3 g). This method (i.e., casting of elastomer and paper coating) is versatile and it allowed fabricating an active 3D origami structure capable of movements in different directions. Moreover, to achieve both linear movements and high actuation force upon vacuum pressure, Zaghoul et al. presented Origami-inspired Semi-soft Pneumatic Actuators (OSPAs) based on the accordion and Yoshimura patterns [63]. For the OSPA with the accordion patterns, a high contraction ratio of 36% and blocking force of 124 N were achieved at a vacuum pressure of -80 kPa. Unlike the conventional Yoshimura pattern, a new design principle was introduced by modifying the Yoshimura pattern [43]. The cross section has a unique configuration as an equilateral triangle, as shown in **Figure 3b**. These morphological features allowed not only the thin film to be folded in an even and ordered manner, but also the actuator to produce a large contraction ratio of up to 99.7%, with a high blocking force of 40 kgf at a vacuum pressure of 60 kPa.

In summary, the Yoshimura patterns enable active 3D origami actuators capable of high deformability and blocking force. These mechanical features are certainly useful to achieve highly versatile and robust soft machines. Moreover, also sensory integration has been investigated. Indeed, Shen et al. embedded optical sensing solution into the origami-inspired PAM (so-called Soft Origami Optical-Sensing Actuators (SOSAs)) and presented a hybrid underwater 3-DoFs manipulator [59].

2.2.2 Miura-Ori patterned unit cell

The Miura-Ori pattern, introduced by Japanese Kogyo Miura, represents a folding technique consisting of congruent parallelograms forming a zigzag configuration in two directions [64, 65] (**Figure 3c**). The Miura folding enables high stiffness, compressibility, and extensibility [66]. Its geometry plays a key role in the mechanical properties of the folded metamaterial, exhibiting a negative Poisson's ratio between the two planar degrees of freedom [67]. Due to such extraordinary mechanical characteristics, this folding pattern was employed for the packaging and deployment of

large membranes in space, such as foldable maps or solar panel deployment [68, 69]. From the architecture point of view, two different approaches are available to achieve desired linear deformations—1) a single planar Miura-Ori sheet mainly due to in-plane kinematics; or 2) a 3D folding structure (i.e., bellow) mainly due to out-of-plane kinematics.

As regards in-plane kinematics, Li et al. presented a surface (2D) skeleton made of a standard Miura-Ori pattern and demonstrated its high compressibility of up to 92% upon vacuum pressure [57], as shown in **Figure 3d**. Moreover, by exploiting asymmetrical out-of-plane motions, a 2D Miura-Ori skeleton was capable of complex motions combining both torsion and contraction. For the 3D folding structures, Reid et al. explored the bistability of the bellow pattern with the Miura-Ori folds and presented a promising technique, enabling arbitrarily complicated bellows with finely tuned fold parameters [70]. To achieve a compressible 3D structure, each bend should be paired, and thus the number of bends was even. Another example is the monothetic foldable part composed of two Miura-Ori units combined up and down. Yu et al. introduced pneumatic foldable actuators (PFAs) capable of biaxial movements upon vacuum and positive pressures [66]. This way, the compression of up to 43% was achieved at -10 kPa. However, the extensibility was limited down to 19% at 10 kPa. It is noted that the movements were mainly dependent on the length change by the folding of the actuator at low vacuum pressure, rather than the volumetric changes by positive pressure.

2.2.3 Kresling patterned unit cell

The Kresling pattern consists of a series of parallel diagonal creases defined by triangular facets [71, 72] (see **Figure 3e**). Such triangulated cylinder pattern enables bistable movements (i.e., contraction and elongation) facilitated by the buckling of the thin wall [73] while ensuring the fully foldable structure. However, this approach could suffer from mechanical failures (i.e., unbalanced deployment), resulting in coupled longitudinal and rotational motions. In principle, the work (W) required for each rotational step can be defined as a function of the elastic energy associated with axial stiffness (K_{axial}) and torsion stiffness ($K_{rotational}$). Thus, as shown in **Figure 3e**, Pagano et al. derived the overall structure stiffness given by a function of variations in rotation angle (α) and the height (H) [73], as follows:

$$K_{axial} = \frac{W^2}{\Delta H^2}, \quad K_{rotational} = \frac{W^2}{\Delta \alpha^2} \quad (6)$$

Due to bistability, the actuators are generally capable of axial deformations together with coupled rotational motions *via* different core actuation sources (i.e., pneumatic [44, 74], tendon [75], magnetic [76], Shape Memory Alloy (SMA) [71], etc.). To the authors' knowledge, very few studies have demonstrated pneumatic actuators based on the Kresling pattern. Zhang et al. presented a Pneumatic and Cable-driven hybrid Linear Actuator (PCLA) capable of both thrust and tensile force [74]. The PCLA can be fully deployed (up to 200%) with a low input pressure of 2 kPa at null load and generates high force up to 70 N at 10 kPa. Herein, the diagonal creases play a crucial role in making both axial and torsional movements only for the single-story origami chamber. In this view, Vacuum-powered Soft Pneumatic Twisting Actuators (V-SPTAs) designed by adopting the diagonal creases at the single chamber could belong to the Kresling pattern class [44]. The V-SPTA was

capable of high contraction force and torque. Its mechanical performance can be tunable depending on geometric parameters (i.e., initial height and initial rotation angle). For the multiple chambers, such as origami stories, the even number with reversed diagonal creases can counterbalance the rotational motions that occur at each chamber. This approach enabled the development of a 3D-printed origami V-PAM capable of pure axial movement [58], as shown in **Figure 3f**. Due to the rigid inner support rings interfaced at each module, the radial contraction can be avoided, resulting in a high compression ratio of 62% with 3 kgf payload upon vacuum pressure.

2.2.4 Origami-skeleton structure

In origami-skeleton structures, zigzag patterned structure is exploited, as a skeleton made of minimally extensible materials, such as air-tight fabrics and polyethylene [57, 77]. In principle, these compressible skeletons incorporate collapsible structures inspired by origami and/or mechanical springs. Hence, although the skin enveloping the skeletal structure has no morphological features (i.e., bellow or pleated skin), the linear movement is mainly due to the compressible skeletons. More in detail, the vacuum pressure enables the volume inside the film pouch to be evacuated, and it induces a controlled collapse in the direction guided by the skeletal structure [78]. With these findings in mind, Li et al. introduced design principles that enable linear movements and presented Fluid-driven Origami-inspired Artificial Muscles (FOAMs) by exploiting symmetrical zigzag geometry [57]. They investigated the mechanical performance of the FOAMs based on different design parameters and concluded that the maximum contraction ratio can be achieved by exploiting thin zigzag skeletons. Indeed, for the nylon fabric pouches with 0.34 mm thickness, the actuator has shown 50% linear contraction with a blocking force of 201 N. In the case of a thinner film made of polyester material (0.038 mm, with a skeleton thickness of 0.254 mm), an ultralight FOAM (2.6 g) was capable of a blocking force of up to 3 kgf, as shown in **Figure 3g**. Based on these design principles, Oguntosin et al. developed artificial muscles completely made of soft silicone rubber without any rigid parts [79]. A maximum contractile strain of 67% was achieved upon null load and a vacuum pressure of 34.5 kPa.

Another approach consists in exploiting a mechanical compression spring. Kulasekera et al. presented a Low-Profile Vacuum Actuator (LPVAc) by low-profile spring encased within a polyethylene film pouch that contracts longitudinally when vacuum pressure is applied [80]. This study highlighted that actuation was strongly dependent on the mechanical characteristics of the low-profile spring, and a high force-to-weight ratio was achieved. Indeed, the LPVAc was only 14 g, yet a high contractile strain of 65% and blocking force of 2.2 kgf (that corresponds to 160 times its own weight) were achieved. The same research group extended further this work. An airtight pouch made of a TPU (thermoplastic polyurethane) coated fabric was interfaced with a helical spring skeleton. Hence, the overall weight was reduced down to 2 g, and a high-force-weight ratio (230) was obtained [81]. More recently, they proposed a Thin-walled Vacuum Actuator (ThinVAc) and developed a multi-filament actuator, allowing simple scaling of actuation force while retaining the ability to actuator during deformation [78]. Finally, the weight of the ThinVAc was only 1 g and capable of 60% linear contraction and blocking force of 5.2 N upon null load. Thus, an extremely high force-to-weight ratio of 477 was achieved.

The research on these skin-skeleton designs, demonstrating that low weight and large force-to-weight ratio are achievable, led several researchers to develop them

further for wearable applications. In particular, in the rehabilitation field of infants (of six months or younger), Mendoza et al. optimized the zigzag patterned skeleton. They presented a Low-Profile Vacuum-Powered Artificial Muscle (LP-VPAM) capable of a 61% linear contraction ratio, with a lifting force of 26.4 N at a low vacuum pressure of 40 kPa [77]. Similarly, the LPVAc has shown strong potential for exploiting them in Sit-To-Stand (STS) motion assistance [80, 82].

2.3 Structural instability

Mechanical instabilities in soft PAMs and V-PAMs induce a column squirm (also called buckling), which are considered as mechanical failures in rigid body structures, and result in sudden and significant geometric changes [48, 83–85]. However, in soft robotics structural instabilities can be fruitfully exploited, and this approach shows promising results enabling new functionalities [84, 86]. Indeed, it has been reported that a reversible buckling in assemblies of elastomeric beams or films can be exploited at a variety of soft robots' applications, for example, stretchable soft electronics [87, 88], tunable metamaterials [89–91], or actuators [92]. More importantly, it is remarkable that a structure buckling allows instantaneously trigger large changes in internal pressure, deformation, shape, and exerted force [93].

In this view, it has been shown how a vacuum-driven actuator exploiting a structural instability can achieve an axial deformation due to reversible and cooperative buckling of the beams, enabling an anisotropic change in the shape of the structure [92]. More in detail, such Vacuum-Actuated Muscle-inspired Pneumatic structure (VAMP) was capable of a large longitudinal contraction (up to 40%) with a smaller horizontal deformation (5%), as shown in **Figure 4a**. Yang et al. expanded this work to develop a Shear Vacuum Actuated Machine (Shear-VAM) capable of a linear motion that works by converting the vacuum pressure, applied perpendicularly to its inextensible lateral surfaces, to a force parallel to them *via* tilted elastomeric beams [35], as shown in **Figure 4b**.

Another example is to exploit the characteristics of foams and elastomers. Roberston et al. presented a Vacuum-powered Soft Pneumatic Actuator (V-SPA) and developed 3-DoFs robotic platform [94]. A particular geometry (see **Figure 4c**) that allows inward compression and buckling of the side walls were employed to avoid possible interferences that could limit the actuator's strokes. For a single module, the V-SPA was capable of generating a blocking force of 0.92 N upon vacuum pressure of 35 kPa [34].

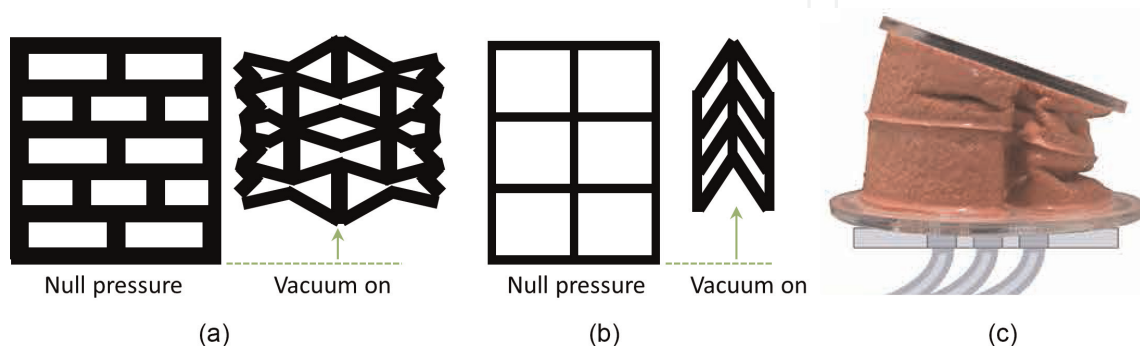


Figure 4. (a) and (b) working principles of vacuum-powered Pneumatic Artificial Muscle (VAMP) exploiting a structural instability [92] and of Shear Vacuum Actuated Machine (Shear-VAM) [35]. (c) 3 DoFs robotic platform interfaced with vacuum-powered Soft Pneumatic Actuators (V-SPA). Reproduced with permission [94].

3. Fabrication and materials

The manufacturing process is an essential, yet delicate, step in the implementation of soft pneumatic actuators. However, from the manufacturing point of view, there are no significant differences among vacuum-powered or inflatable fluidic actuators.

Depending on the design principles, there are several approaches to fabricate V-PAMs, and an adequate fabrication protocol should ensure high reproducibility and repeatability. Due to the rapid development in additive manufacturing, modern techniques (e.g., stereolithography or multi-material 3D printing, etc.) are currently available, which enable the direct fabrication of the actuators with a good trade-off between material consumption and cost-effectiveness. Moreover, such additive manufacturing techniques are also widely used to fabricate molds and active elements typical of the hybrid manufacturing approach.

In this section, the fabrication approaches that are commonly used for implementing V-PAMs are overviewed (with mention to the employed materials), including molding manufacturing, additive manufacturing, and hybrid techniques. Their advantages and limitations are discussed and compared.

3.1 Molding manufacturing

Molding manufacturing is defined as the process of shaping a liquid or a raw material using a rigid container called mold or matrix, which has a negative geometry of the desired shape. Due to the advent of 3D printing, laser cutting, and CNC milling, fabricating the mold has become affordable and relatively fast. Here, depending on the complexity of the object, different molding approaches need to be considered (i.e., casting, blow molding, injection molding, etc.), while only a few of them have been widely addressed to produce soft actuators. In literature, it is frequent to find examples of inflatable fluidic actuators [95–98] and vacuum-powered actuators [44, 92, 99] mainly built *via* casting or injection molding. Generally, in both approaches, due to the shape complexity of vacuum actuators, articulated molds, and multiple steps are required. To better understand these molding techniques, and to describe some relative case studies for V-PAMs, three main phases in fabrication need to be considered—mold design and fabrication, molding, demolding, and assembly.

A correct design and construction of the mold is the first step to succeed in this process. A good practice is to design the mold to be reusable while simplifying the demolding phase and avoiding material waste due to sacrificial molds. This way the risk of damaging the samples during extraction is minimized. To this aim, materials used for the mold should be investigated, taking into account their compatibility with casting materials, and curing parameters. Given that soft actuators are generally built from silicon-rubber or urethane-based silicon, then Acrylonitrile butadiene styrene (ABS), PolyTetraFluoroEthylene (PTFE), PolyAmide (PA), and Chlorinated PolyEthylene (CPE) are good candidates for the molds. Alternatively, PolyLActide (PLA) could be used, while curing elastomers can be completed only at room temperature due to its thermomechanical characteristics (e.g., glass transition temperature T_g).

The second step is to pour the elastomers into the mold and to determine an adequate curing process with specific temperatures and timing. As shown in **Figure 5a**, based on the mold filling methodology, either casting (where the liquid material is driven by gravity in the mold cavities), or injection molding (where the material is forced into the mold by pressurization) can be used. Once the mold is filled, it must be

placed in a vacuum chamber to remove air bubbles that would instead remain trapped in the cured material affecting the final mechanical characteristics of the same.

The last step is to extract the cured parts without any damage. Where proper mold design is insufficient to ensure a correct extraction, synthetic lubricants (e.g., Teflon coating) can help to avoid failures (e.g., delamination at bonded layers). Finally, once all components are ready, the actuators are assembled in the desired configuration by using uncured materials or silicone adhesives.

With the aforementioned procedures in molding fabrication, Balak et al. developed a vacuum-powered omnidirectional soft robotic actuator (OSRA) [99]. A two-step molding process was employed. The core structure and cavities of the OSRA were first obtained by using three mold parts. Once the first part was cured, the actuator was completed by putting the cured part into a second mold to make the base seal. Similarly, in ref. [44], the authors employed the molding fabrication technique and could obtain a vacuum soft pneumatic twisting actuator (V-SPTA). First, the body and bottom parts of the V-SPTA were made by casting and, in a second step, attached through a silicone adhesive layer. The same two-step procedure was applied to

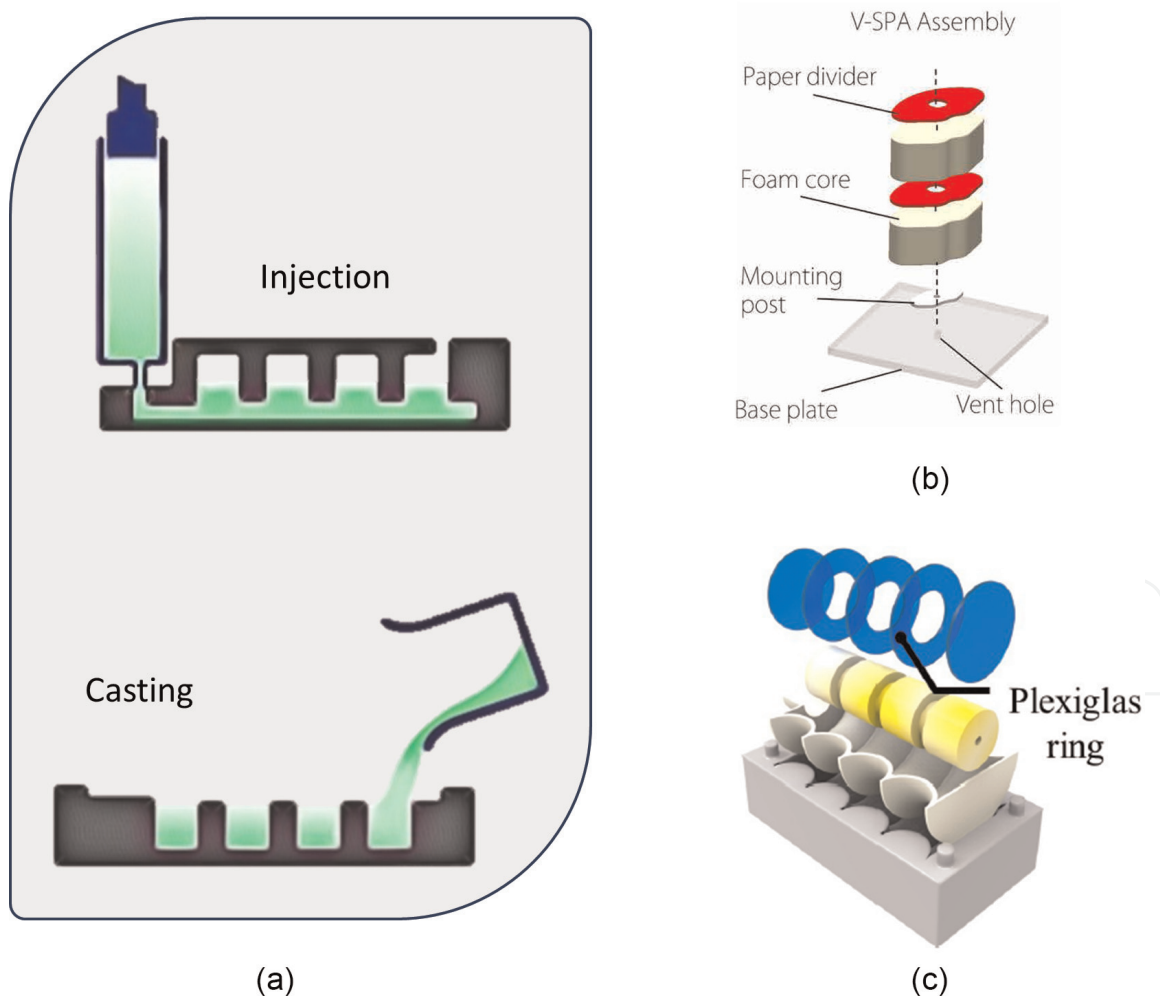


Figure 5. Different fabrication techniques. (a) shows different filling methodologies - Injection and casting molding, respectively. The hybrid fabrication processes combining two or more techniques - (b) encasing the foam core with the elastomer and smoothly merging each module by interfacing paper dividers. Reproduced with permission [94]. (c) a bellow type actuator (UH-PAM [38]) with foam modules and Plexiglas® rigid rings interfaced at each convolution of the elastomeric bellow skin [38].

fabricate the buckling actuators shown in refs. [44, 58, 79, 92, 99]. However, the silicone curing was performed in a controlled environment at 60°C for 10 minutes, reducing the fabrication time. Finally, Oguntosin and Akindele [79] show a remarkable example of a soft vacuum actuator fabricated entirely from silicon rubber. The approach followed the molding method, but unlike the previous examples [44, 79, 99], two different elastomeric materials were smoothly interfaced in one final structure.

3.2 Additive manufacturing

Additive manufacturing (AM), also known as three-dimensional (3D) printing, encompasses several emerging techniques based on the same principle: starting from a 3D model, replicate the structure by sequentially adding layers of material until model completeness. In literature, different fabrication protocols have been investigated to obtain soft actuators operated by either positive [100–104] or negative pressure [37, 105, 106].

Table A2 (in the Appendix) summarizes different AM processes defined by ISO/ASTM 52900:2021. Of these, only Vat PhotoPolymerization (VPP), Material EXtrusion (MEX), and Material Jetting (MJT) have been widely used in the production of soft actuators [107]. In particular, Fused Filament Fabrication (FFF) is the most widely used MEX technology in soft robotics. In this process, a continuous filament of thermoplastic material is melted and extruded through a nozzle to form the horizontal layers of the 3D structure [108, 109]. Using the same principle, in Direct Ink Writing (DIW), a liquid-phase ink is arranged along the horizontal path, defining the 3D structures layer by layer [110].

On the VPP side, Digital Light Processing (DLP) and Stereolithography (SLA) are commonly subjected. Both use photopolymer resin, differing curing methods [109, 111]. The DLP printer uses a digital light projector screen that flashes an image of the layer that defines the surface to be cured. In contrast, the SLA employs a laser to draw and cure the layer following the surface pattern. Unlike FFF, parts obtained with DLP and SLA need adequate post-processing to achieve optimal material properties. First, all components should be gently removed. Then, the excess resin is removed by using ethanol (bio) or isopropyl alcohol, preferably with ultrasound or under agitation. Once the supports are removed, the last step requires a post-curing step under high-power UV for a few minutes at about 65°C.

Finally, among MJT processes, PolyJet is the typical approach used. PolyJet relies on a sequential deposition of material droplets like an inkjet printer. First, photopolymer droplets are accumulated to form the layer, then instantaneous exposure to UV light cures the layer before a new one is deposited [112]. Stano et al. recently classified the AD approaches employed to fabricate soft robots in rapid mold manufacturing, hybrid, and total additive manufacturing [107].

In rapid mold manufacturing, the AM limits the production of the mold. The material used in this process does not define the properties of the actuator, which instead are linked to the casted material in a second phase, usually silicone or elastomer. The FFF is the standard technique used in this approach, and ABS and PLA filaments are the typical materials used. The resolution of the 3D printer plays an essential role in the presence of small details. Hence, even though there can be inherent shortcomings (e.g., the high cost of the printing system, the post-processing steps), professional 3D printers are preferred due to the higher resolution along the

z-axis. Indeed, DLP or SLA techniques have been used, to implement complex structures that need to be fabricated with high precision.

Furthermore, the hybrid approach combines AM technologies with traditional manufacturing approaches. Unlike in molding, the elements printed with this approach are embedded in the final object and influence the kinematics of the actuators.

Total Additive Manufacturing (TAM) has attracted much interest in fabricating soft actuators. In this approach, only AD techniques are exploited. Depending on the actuator's complexity, the TAM could follow either a modular or monolithic approach. For the former, all "modules" are printed separately and assembled into the final configuration only in a second step, whereas the latter involves TAM to obtain the actuator by a single printing cycle. Combined with multi-material 3D printing, monolithic TAM allows printing actuators made of two or more materials in a single cycle. The same approach permits embedding sensing elements in actuators, enhancing the mechanical synergy between sensing and movements. In parallel to selecting adequate printing methods among MEX, VPP, and MJT, the material properties need to be considered to accomplish desired mechanical performance. Otherwise, custom-made printers could be developed. Indeed, Byrne et al. proposed a custom setup to exploit the advantages of multi-material 3D printing [113]. Combining fused deposition modeling and a paste extrusion printer, they fabricated soft actuators capable of contracting, bending, or twisting in a single printing run. Similarly, by exploiting a commercial multi-material 3D printer (Ultimaker S3), Stano et al. presented a monolithic bending PneuNets made of TPU 80A and TPU 95A [114].

More recently, the TAM approach has been successfully applied to fabricate vacuum-driven actuators by using fused filament fabrication. In ref. [106], Tawk et al. proposed a bioinspired 3D printable Soft Vacuum Actuators (SOVAs). They showed the versatility functionalities of the AM fabrication by demonstrating various robotic applications (i.e., locomotion robots, grippers, and artificial muscles), by applying both monolithic and modular approaches. Similarly, they presented a Linear Soft Vacuum Actuator (LSOVA) fabricated in a single step using an open-source 3D printer and a commercial TPU filament NinjaFlex (NinjaTek, USA) [37], as shown in **Figure 2d**. While SOVA and L-SOVA are bellow-like and linear vacuum actuators, respectively, the solution proposed by Zhang et al. in [58] is a fully 3-D printed origami-inspired VPAM. Same as molding manufacturing, this demonstrates the versatility of the AM approach, which makes it suitable for different designs.

In summary, the success rate in fabrications exploiting AM is mainly dependent on determining adequate printing parameters. Indeed, an error that could occur at the beginning phase of printing significantly affects the entire process, resulting in printing failures. In particular, for FFF, the bed temperature should be identified to ensure proper layer adhesion without overheating the first layer. At the same time, the size of the first layer should be chosen to accomplish the best quality and airtightness. Avoiding high or low retraction values may help prevent under-extrusion or printed residue. Extrusion temperature, printing speed, and cooling speed deeply affect layer bonding, thus the quality and integrity of the printed part. Finally, an infill density related to the overall structure stiffness enables determining the strength of actuators.

3.3 Hybrid and alternative manufacturing

Hybrid manufacturing combines two or more fabrication techniques. Typically, a tradeoff between 3D printing and other fabrication processes, such as molding manufacturing, is addressed. Qi et al. encapsulated 3D-printed elements made of

custom material into a silicone structure obtained through mold fabrication [115]. Similarly, in ref. [116], a soft actuator with stiffness and shape modulation was obtained by embedding a 3D-printed Conductive PolyLactic Acid (CPLA) layer in a soft pneumatic actuator made of silicone. Robertson et al. in refs. [94, 117] fabricated a V-PAMs without employing molding and additive manufacturing, as shown in **Figure 5b**. First, by using a laser cutting machine, the foam chambers and rigid layers were cut. Then, by gluing them, the core structure of the actuator was assembled, manually coated, and sealed by using Elastosil M4601. **Figure 5c** shows the hybrid fabrication process proposed by the authors in order to develop the UH-PAM [48] (described in Section 2.1.1). Unlike previous examples, after patterning by laser cutting, the open-cell foams (Polyurethane) were integrated with Plexiglass® rigid rings, and with a silicone (Dragon Skin™ 30) skin having a bellow structure, previously molded by casting. Another example belongs to a completely hybrid concept compromising rigid and soft materials [78, 81]. In the V-PAM fabrication, a helical spring core was combined with a pouch, manually assembled from polyethylene (PE) film or TPU fabric. These studies show that hybrid manufacturing has a strong potential, to break down the barrier between rigid and soft materials and to allow them interfacing.

Despite the promising mechanical performance that the hybrid approach delivers to the soft actuators, it suffers from a decreased process controllability since a higher number of separate, and usually manual, fabrication steps are needed, resulting in reduced repeatability and reproducibility. For example, in refs. [78, 81], the repeatability, thus the homogeneity of two different actuators, cannot be ensured since both depend on the manual skills of the operator. Similarly, in ref. [94, 117] using a manual deposition of the core, the homogeneity of the silicone layer could be unevenly distributed.

3.4 Materials

In addition to exploring fabrication protocols, selecting adequate soft materials is a key enabler for soft robot bodies. Although the meaning of the term “soft” has been contentious, in literature soft robots are defined as systems composed of materials with Young’s modulus ranging from 10 kPa to 1 GPa, similar to soft biological materials (i.e., skin or muscle tissue) [118]. In this view, V-PAMs can consist of a wide range of materials (i.e., polymer, rubber-like silicone) that exhibit hyperelastic behavior with a large deformation ratio, or inextensible thin layered materials (i.e., paper, fabric) that could belong to both soft and rigid materials. In this section, some highlights to address an adequate selection of the materials are provided, referring to the main material candidates that are interesting for the fabrication of V-PAMs.

Given that soft materials strongly influence the actuator mechanical properties as well as its kinematic behavior, selecting adequate materials is mainly driven by the predicted deformations (and stresses) that are required along the overall structure. To this aim, for the linear motion, implicit (i.e., Finite element method (FEM)) or explicit numerical approaches (e.g., Euler beam theorem based) were employed to predict desired kinematic trajectories versus input vacuum pressure [119–122]. Moreover, for a V-PAM to achieve high compliance, in addition to the skin material intrinsic compliance, air impermeability is necessary. From the material point of view, elastomeric polymers or silicones can withstand large deformations, in some cases like EcoFlex™ 00-30 up to 900%, without undergoing permanent plastic deformation. Moreover, both air impermeability and compliance can be obtained by exploiting compositions and depositions [123, 124].

As representative solutions, silicones and urethane-based rubbers can be used to realize V-PAMs where molding fabrication is employed. For those hyperelastic constitutive materials, two components (i.e., elastomers, catalyst, or hardener) are mixed at precise mixing ratios (typically 1:1) before degassing and curing. From the mechanical point of view, different elongation at break and Young's modulus can be achievable, depending on materials. For example, platinum-catalyzed silicones (EcoFlex™, DragonSkin™, etc.) are commercially available and exhibit elongation at break ranging from 800% to 1,000% and Young's modulus ranging from few hundreds kPa to 50 MPa; whereas the mechanical characteristics of Polydimethylsiloxane (PDMS, Sylgard184) can be tuned by using different elastomer/cross-linking agent ratio (e.g., 10:1, 20:1, 30:1).

As regards additive manufacturing, filaments of TPU, such as NinjaFlex® TPU or Ultimaker TPU, are the most used to fabricate soft actuators (including both inflatable fluidic actuators and V-PAMs) by the TAM approach. In general, TPU filaments are characterized by hardness in the 75–90 Shore A range, with an elongation at the break that could reach almost 700%. Alternatively, the Thermoplastic Polyether-Polyurethane elastomer, such as the Recreus FilaFlex, shows a similar characteristic, offering elongation at break up to 950% and hardness in the range 60–95 shore A.

Table 1 provides a brief overview of some of the most common materials used in the fabrication of V-PAMs. In terms of elongation at break, both silicone and filaments offer good performance, showing values that can range from 100% up to a maximum of 1000%. On the contrary, from the point of view of Young's modulus, the V-PAM obtained with silicone shows values 10 times lower than the counterpart obtained with the TAM approach. This means that for the same structure, actuators obtained by casting are always softer than those obtained by 3D printing, which resulting more rigid require, an higher actuation power to achieve the same behavior. On the other hand, higher stiffness can lead to solutions that can support a higher payload. For this reason, the choice of material is a compromise between performance, feasibility of the concept and operating conditions. The latter point in particular makes it difficult to define a priori which material is best based on the design used alone, making careful analysis necessary in the design phase.

4. Conclusion and outlook

This review introduces the promising potential of V-PAMs for implementing complex soft machines achieving robustness and fail-safe operation. In contrast to the inflatable fluidic actuators, given that vacuum pressure induces a volumetric contraction, the linear deformation is strongly influenced by the contraction in the radial direction. Thus, their structures and geometries can avoid stiffening and/or an increase in stress during movement, at the same time ensuring a good level of compactness and robustness. In particular, due to their reliability [37, 92, 106], the V-PAMs proposed to show a lifespan that varies from a minimum of 21,500 cycles of LSOVAs up to more than 1,000,000 cycles of VAMPs. Furthermore, being based on volumetric contraction, V-PAMs results suitable for operating in both large and limited spaces, oppositely to PAMs, which exploiting a volumetric expansion cannot properly work in confined environments.

Nevertheless, there are still several open challenges to be addressed. Indeed, new trade-offs among design principles and desired mechanical performance need to be

found to enable energy efficiency in actuators with high power-to-weight ratio. Also, scalability remains barely impossible, mainly due to the square-cube law.

Given that upon vacuum pressure, the overall structure stiffness is mainly dependent on its bulk state, determining adequate materials is a key aspect to achieve the desired actuation force. Thus, exploiting different materials (multi-material) approaches that allow for enhancing the axial stiffness at a global level have been widely addressed [125–128] by smoothly interfacing them with the structure. However, this approach could lead to an increase in the overall structure weight, as well as material failures (i.e., delamination). Thereby, there is the quest for new materials and/or investigation of novel design principles.

An interesting approach is to employ foam (like in the UH-PAM [38]) as a constituent material, or porous structures where the air-cells dimensions can be decided upon the desired stiffness. Notably, given the recent advances in foam-like sensing,

	Young's module [MPa]	Shore hardness [A]	Elongation at break [%]	Manufacturing		
				Molding	Additive	Hybrid
Silicones						
Ecoflex™ 00-10	0.55	10	800	•		•
Ecoflex™ 00-20	0.55	20	845	•		•
Ecoflex™ 00-30	0.69	30	900	•		•
DragonSkin™ 10,	0.151	10	1,000	•		•
DragonSkin™ 20,	0.338	20	620	•		•
DragonSkin™ 30,	0.593	30	364	•		•
Sylgard 184 (10:1)	1.32	43	100	•		•
Elastosil® M4601	0.262	28	700	•		•
Filament (TAM)						
Ultimaker TPU	26	95	580		•	•
NinjaFlex© TPU	12	85	660		•	•
Chinchilla™ TPE	34	75	600		•	•
FilaFlex 60A (TPU)	26	63	950		•	•
FilaFlex 82A (TPU)	22	82	650		•	•
FilaFlex 70A (TPU)	32	70	900		•	•
	Young's module [GPa]	Shore hardness [D]	T _g [°C]	Manufacturing		
				Molding	Additive	Hybrid
Filament (molds)						
Ultimaker ABS	1.618	76	90–105		•	•
Ultimaker CPE+	1.128	75	90–110		•	•
Ultimaker PLA	2.346	83	55–65		•	•
PolyLite™ ABS	2.174	—	101		•	•
PolyLite™ PLA	2.636	—	63		•	•

Table 1. Materials' properties and the compatibility with different V-PAMs manufacturing.

(e.g., capacitive [129], inductive sensing [130], resistive sensing [131, 132], etc.), it can be construed that, in a near future, new designs should consider such transduction mechanisms embedded in V-PAMs. This approach seems promising to develop soft machines with embodied intelligence *via* proprioceptive and/or exteroceptive sensory feedback [133].

Indeed, due to the rapid development in additive manufacturing, designing and fabricating 3D architectures made of metamaterials has been demonstrated [134–137]. Hence, it can be expected for them to play a key role in the future development of soft actuation, allowing the soft machines to exhibit desired kinematic performance while reducing overall weight due to the tessellated topology and morphology. For this to happen, the quest is for materials that possess high extensibility (>500%), Young’s modulus in the range of tens of MPa, and high reliability and low hysteresis.

In conclusion, in any case, it will be important to address designs that exploit both positive and negative pressures, rather than choosing one of them. This way motions in different directions could be achieved with the same actuator, for example, elongation, contraction, bending, twisting, also inspiring from natural models. For example, this is the case of developing innovative continuum manipulators inspired from elephant trunks, like in the EU project PROBOSCIS [138], which aim is to develop “soft” yet “strong” perceptive soft machines.

Acknowledgements

This work has received funding from the European Union’s Horizon 2020 research and innovation program under grant agreement No. 863212 (PROBOSCIS project).

Conflict of interest

The authors declare no conflict of interest.

Appendices and nomenclature

Nomenclatures	Descriptions	Nomenclatures	Descriptions
D	Outer diameter	TPU	Thermoplastic polyurethane
d	Inner diameter of the bellow	PDMS	Polydimethylsiloxane
D_m	Mean diameter of the bellow	PE	Polyethene
w	Convolution depth	AM	Additive Manufacturing
E_b	Young’s modulus of the material used for the bellow	VPP	Vat Polymerization
t_p	Thickness of skin	MEX	Material Extrusion
μ	Poisson’s ratio	MJT	Material Jetting
n	Number of bellow plies (in case of multiple plies)	DLP	Digital Light Processing
N	Number of convolutions	SLA	Stereolithography

Nomenclatures	Descriptions	Nomenclatures	Descriptions
ABS	Acrylonitrile butadiene styrene	FFF	Fused Filament Fabrication
PTFE	Polytetrafluoroethylene	DIW	Direct Ink Writing
PA	Polyamide	TAM	Total additive manufacturing
CPE	Chlorinated polyethylene	T _g	Glass transition temperature
PLA	Poly lactide		

Table A1.
Nomenclatures.

Process name	Operative principle
Binder Jetting (BJT)	A liquid bonding agent is selectively deposited to join powder materials
Direct Energy Deposition (DED)	Focused thermal energy is used to fuse materials by melting as they are being deposited
Material Extrusion (MEX)	Material is selectively dispensed through a nozzle or orifice
Material Jetting (MJT)	Droplets of feedstock material are selectively deposited
Powder Bed Fusion (PBF)	Thermal energy selectively fuses regions of a powder bed
Sheet Lamination (SHL)	Sheets of material are bonded to form a part
Vat Photopolymerization (VPP)	Liquid photopolymer in a vat is selectively cured by light-activated polymerization
Binder Jetting (BJT)	A liquid bonding agent is selectively deposited to join powder materials
Direct Energy Deposition (DED)	Focused thermal energy is used to fuse materials by melting as they are being deposited
Material Extrusion (MEX)	Material is selectively dispensed through a nozzle or orifice
Material Jetting (MJT)	Droplets of feedstock material are selectively deposited
Powder Bed Fusion (PBF)	Thermal energy selectively fuses regions of a powder bed
Sheet Lamination (SHL)	Sheets of material are bonded to form a part
Vat Photopolymerization (VPP)	Liquid photopolymer in a vat is selectively cured by light-activated polymerization

Table A2.
Different printing processes and their operation principles.

IntechOpen


IntechOpen

Author details

Seonggun Joe, Federico Bernabei and Lucia Beccai*
Istituto Italiano di Tecnologia, Genova, Italy

*Address all correspondence to: Lucia.beccai@iit.it

IntechOpen

© 2022 The Author(s). Licensee IntechOpen. This chapter is distributed under the terms of the Creative Commons Attribution License (<http://creativecommons.org/licenses/by/3.0>), which permits unrestricted use, distribution, and reproduction in any medium, provided the original work is properly cited. 

References

- [1] Xu W, Chen J, Lau HY, Ren H. Data-driven methods towards learning the highly nonlinear inverse kinematics of tendon-driven surgical manipulators. *The International Journal of Medical Robotics and Computer Assisted Surgery*. 2017;**13**(3):e1774
- [2] Kastor N, Mukherjee R, Cohen E, Vikas V, Trimmer BA, White RD. Design and manufacturing of tendon-driven soft foam robots. *Robotica*. 2020;**38**(1): 88-105
- [3] Pabst O, Hölzer S, Beckert E, Perelaer J, Schubert US, Eberhardt R, et al. Inkjet printed micropump actuator based on piezoelectric polymers: Device performance and morphology studies. *Organic Electronics*. 2014;**15**(11): 3306-3315
- [4] Kofod G, Wirges W, Paajanen M, Bauer S. Energy minimization for self-organized structure formation and actuation. *Applied Physics Letters*. 2007; **90**(8):081916
- [5] Ji X, Liu X, Cacucciolo V, Imboden M, Civet Y, El Haitami A, et al. An autonomous untethered fast soft robotic insect driven by low-voltage dielectric elastomer actuators. *Science. Robotics*. 2019;**4**(37):eaaz6451
- [6] Akbari S, Sakhaei AH, Panjwani S, Kowsari K, Serjouei A, Ge Q. Multimaterial 3D printed soft actuators powered by shape memory alloy wires. *Sensors and Actuators A: Physical*. 2019; **290**:177-189
- [7] Huang X, Kumar K, Jawed MK, Mohammadi Nasab A, Ye Z, Shan W, et al. Highly dynamic shape memory alloy actuator for fast moving soft robots. *Advanced Materials Technologies*. 2019;**4**(4):1800540
- [8] Lendlein A. Fabrication of reprogrammable shape-memory polymer actuators for robotics. *Science. Robotics*. 2018;**3**(18):eaat9090
- [9] Ma S, Zhang Y, Liang Y, Ren L, Tian W, Ren L. High-performance ionic-polymer-metal composite: Toward large-deformation fast-response artificial muscles. *Advanced Functional Materials*. 2020;**30**(7):1908508
- [10] Festo. TentacleGripper 2022. Available from: https://www.festo.com/us/en/e/about-festo/research-and-development/bionic-learning-network/highlights-from-2015-to-2017/tentaclegripper-id_33321/?siteUId=fox_us&siteName=Festo+USA
- [11] Robotics S. mGrip 2022. Available from: <https://www.softroboticsinc.com/products/mgrip-modular-gripping-solution-for-food-automation/>
- [12] Polygerinos P, Wang Z, Galloway KC, Wood RJ, Walsh CJ. Soft robotic glove for combined assistance and at-home rehabilitation. *Robotics and Autonomous Systems*. 2015;**73**: 135-143
- [13] Nguyen PH, Zhang W. Design and computational modeling of fabric soft pneumatic actuators for wearable assistive devices. *Scientific Reports*. 2020;**10**(1):1-13
- [14] Maeder-York P, Clites T, Boggs E, Neff R, Polygerinos P, Holland D, et al. Biologically inspired soft robot for thumb rehabilitation. *Journal of Medical Devices*. 2014;**8**(2):020933
- [15] Manfredi L, Capoccia E, Ciuti G, Cuschieri A. A soft Pneumatic Inchworm Double balloon (SPID) for colonoscopy. *Scientific Reports*. 2019;**9**(1):1-9

- [16] Okayasu H, Okamoto J, Fujie MG, Umezu M, Iseki H. Development of a hydraulic-driven flexible manipulator for neurosurgery. In: International Congress Series. 2003
- [17] Watanabe Y, Maeda M, Yaji N, Nakamura R, Iseki H, Yamato M, et al. Small, soft, and safe microactuator for retinal pigment epithelium transplantation. In: 2007 IEEE 20th International Conference on Micro Electro Mechanical Systems (MEMS). 2007
- [18] Chen C-Y, May KP, Yeow C-H. 3D printed soft extension actuator. In: IEEE 4th International Conference on Soft Robotics (RoboSoft). 2021
- [19] Shintake J, Rosset S, Schubert B, Floreano D, Shea H. Versatile soft grippers with intrinsic electroadhesion based on multifunctional polymer actuators. *Advanced Materials*. 2016; **28**(2):231-238
- [20] Hao Y, Biswas S, Hawkes EW, Wang T, Zhu M, Wen L, et al. A multimodal, enveloping soft gripper: Shape conformation, bioinspired adhesion, and expansion-driven suction. *IEEE Transactions on Robotics*. 2020; **37**(2):350-362
- [21] Zongxing L, Wanxin L, Liping Z. Research development of soft manipulator: A review. *Advances in Mechanical Engineering*. 2020; **12**(8): 1687814020950094
- [22] Kastor N, Vikas V, Cohen E, White RD. A definition of soft materials for use in the design of robots. *Soft Robotics*. 2017; **4**(3):181-182
- [23] Gollob SD, Park C, Koo BHB, Roche ET. A modular geometrical framework for modelling the force-contraction profile of vacuum-powered soft actuators. *Frontiers in Robotics and AI*. 2021; **8**:606938
- [24] Veale AJ, Xie SQ, Anderson IA. Characterizing the Peano fluidic muscle and the effects of its geometry properties on its behavior. *Smart Materials and Structures*. 2016; **25**(6):065013
- [25] Wang L, Wang Z. Mechanoreception for soft robots via intuitive body cues. *Soft Robotics*. 2020; **7**(2):198-217
- [26] Digumarti KM, Conn AT, Rossiter J. Euglenoid-inspired giant shape change for highly deformable soft robots. *IEEE Robotics and Automation Letters*. 2017; **2**(4):2302-2307
- [27] Goulbourne N, Son S, Fox J. Self-sensing McKibben actuators using dielectric elastomer sensors. In: *Electroactive Polymer Actuators and Devices (EAPAD)*. 2007
- [28] Tondu B, Lopez P. Modeling and control of McKibben artificial muscle robot actuators. *IEEE Control Systems Magazine*. 2000; **20**(2):15-38
- [29] Chou C-P, Hannaford B. Measurement and modeling of McKibben pneumatic artificial muscles. *IEEE Transactions on Robotics and Automation*. 1996; **12**(1): 90-102
- [30] Al-Ibadi A, Nefti-Meziani S, Davis S. The design, kinematics and torque analysis of the self-bending soft contraction actuator. *Actuators*; 2020
- [31] Daerden F, Lefeber D. The concept and design of pleated pneumatic artificial muscles. *International Journal of Fluid Power*. 2001; **2**(3):41-50
- [32] Verrelst B. A dynamic walking biped actuated by pleated pneumatic artificial muscles: Basic concepts and control

issues. PhD Thesis Vrije Universiteit Brussel. 2005

[33] Daerden F, Lefeber D. Pneumatic artificial muscles: Actuators for robotics and automation. *European Journal of Mechanical and Environmental Engineering*. 2002;**47**(1):11-21

[34] Agarwal G, Robertson MA, Sonar H, Paik J. Design and computational modeling of a modular, compliant robotic assembly for human lumbar unit and spinal cord assistance. *Scientific Reports*. 2017;**7**(1):1-11

[35] Yang D, Verma MS, Lossner E, Stothers D, Whitesides GM. Negative-pressure soft linear actuator with a mechanical advantage. *Advanced Materials Technologies*. 2017;**2**(1):1600164

[36] Mott PH, Dorgan JR, Roland C. The bulk modulus and Poisson's ratio of "incompressible" materials. *Journal of Sound and Vibration*. 2008;**312**(4-5): 572-575

[37] Tawk C, Spinks GM, in het Panhuis M, Alici G. 3D printable linear soft vacuum actuators: Their modeling, performance quantification and application in soft robotic systems. *IEEE/ASME Transactions on Mechatronics*. 2019;**24**(5):2118-2129

[38] Joe S, Totaro M, Wang H, Beccai L. Development of the ultralight hybrid pneumatic artificial muscle: Modelling and optimization. *PloS One*. 2021;**16**(4): e0250325

[39] Daerden F. Conception and Realization of Pleated Pneumatic Artificial Muscles and Their Use as Compliant Actuation Elements. Belgium: Vrije Universiteit Brussel; 1999

[40] Immega G, Kukolj M. Axially contractable actuator. Google Patents; 1990

[41] Snedden N. Analysis and design guidance for the lateral stiffness of bellows expansion joints. *Thin-walled Structures*. 1985;**3**(2):145-162

[42] Becht C IV. An evaluation of EJMA stress calculations for unreinforced bellows. *Journal of Pressure Vessel Technology*. 2002;**124**(1):124-129

[43] Lee J-G, Rodrigue H. Origami-based vacuum pneumatic artificial muscles with large contraction ratios. *Soft Robotics*. 2019;**6**(1):109-117

[44] Jiao Z, Ji C, Zou J, Yang H, Pan M. Vacuum-powered soft pneumatic twisting actuators to empower new capabilities for soft robots. *Advanced Materials Technologies*. 2019;**4**(1): 1800429

[45] Yang HD, Greczek BT, Asbeck AT. Modeling and analysis of a high-displacement pneumatic artificial muscle with integrated sensing. *Frontiers in Robotics and AI*. 2019;**5**:136

[46] Hashem R, Stommel M, Cheng L, Xu W. Design and characterization of a bellows-driven soft pneumatic actuator. In: *IEEE/ASME Transactions on Mechatronics*. 2020

[47] Felt W, Robertson MA, Paik J. Modeling vacuum bellows soft pneumatic actuators with optimal mechanical performance. In: *IEEE International Conference on Soft Robotics (RoboSoft)*. 2018

[48] Joe S, Wang H, Totaro M, Beccai L. Development of ultralight hybrid pneumatic artificial muscle for large contraction and high payload. In: *3rd IEEE International Conference on Soft Robotics (RoboSoft)*. 2020

[49] Belforte G, Eula G, Ivanov A, Visan AL. Bellows textile muscle. The

Journal of The Textile Institute. 2014;
105(3):356-364

[50] Smith KK, Kier WM. Trunks, tongues, and tentacles: Moving with skeletons of muscle. *American Scientist*. 1989;77(1):28-35

[51] Casi DV. Development of the production process of PPAM: Ph. D. Thesis, Universidad Publica de Navarra; 2009

[52] Rafsanjani A, Bertoldi K, Studart AR. Programming soft robots with flexible mechanical metamaterials. arXiv preprint arXiv:190600306. 2019

[53] Yoshimura Y. On the mechanism of buckling of a circular cylindrical shell under axial compression. 1955

[54] Chen Y, Peng R, You Z. Origami of thick panels. *Science*. 2015;349(6246):396-400

[55] Paez L, Granados M, Melo K, Conceptual design of a modular snake origami robot. 2013 IEEE International Symposium on Safety, Security, and Rescue Robotics (SSRR); 2013

[56] Onal CD, Wood RJ, Rus D, Towards printable robotics: Origami-inspired planar fabrication of three-dimensional mechanisms. 2011 IEEE international conference on robotics and automation; 2011

[57] Li S, Vogt DM, Rus D, Wood RJ. Fluid-driven origami-inspired artificial muscles. *Proceedings of the National Academy of Sciences*. 2017;114(50):13132-13137

[58] Zhang Z, Fan W, Chen G, Luo J, Lu Q, Wang H, A 3D printable origami vacuum pneumatic artificial muscle with fast and powerful motion. 2021 IEEE 4th

International Conference on Soft Robotics (RoboSoft); 2021

[59] Shen Z, Zhao Y, Zhong H, Tang K, Chen Y, Xiao Y, et al. Soft origami optical-sensing actuator for underwater manipulation. *Frontiers in Robotics and AI*. 2021;7:219

[60] Woerd JD, Chudoba R, Hegger J, Single-curved shell structure made out of textile-reinforced concrete plate using a folding technique. *Proceedings of IASS Annual Symposia*; 2013

[61] Paez L, Agarwal G, Paik J. Design and analysis of a soft pneumatic actuator with origami shell reinforcement. *Soft Robotics*. 2016;3(3):109-119

[62] Martinez RV, Fish CR, Chen X, Whitesides GM. Elastomeric origami: Programmable paper-elastomer composites as pneumatic actuators. *Advanced Functional Materials*. 2012; 22(7):1376-1384

[63] Zaghoul A, Bone GM. 3D shrinking for rapid fabrication of origami-inspired semi-soft pneumatic actuators. *IEEE Access*. 2020;8:191330-191340

[64] Miura K. Method of packaging and deployment of large membranes in space. *The Institute of Space and Astronautical Science Report*. 1985;618: 1-9

[65] Stavric M, Wiltsche A. Investigations on quadrilateral patterns for rigid folding structures—folding strategies—rigid and curved folding. 2013

[66] Yu M, Yang W, Yu Y, Cheng X, Jiao Z, A crawling soft robot driven by pneumatic foldable actuators based on Miura-ori. *Actuators*; 2020

[67] Schenk M, Guest SD. Geometry of Miura-folded metamaterials.

- Proceedings of the National Academy of Sciences. 2013;**110**(9):3276-3281
- [68] Horner G, Elliott M, A fabrication and deployment approach for a Miura-ori solar sail model. 43rd AIAA/ASME/ASCE/AHS/ASC Structures, Structural Dynamics, and Materials Conference; 2002
- [69] Horner G, Wright T, Laue G, Miura-Ori solar sail packaging concept development and deployment demonstration. 39th AIAA/ASME/SAE/ASEE Joint Propulsion Conference and Exhibit; 2003
- [70] Reid A, Lechenault F, Rica S, Addabedia M. Geometry and design of origami bellows with tunable response. *Physical Review E*. 2017;**95**(1):013002
- [71] Nayakanti N, Tawfick SH, Hart AJ. Twist-coupled kirigami cells and mechanisms. *Extreme Mechanics Letters*. 2018;**21**:17-24
- [72] Jianguo C, Xiaowei D, Ya Z, Jian F, Yongming T. Bistable behavior of the cylindrical origami structure with Kresling pattern. *Journal of Mechanical Design*. 2015;**137**(6):061406
- [73] Pagano A, Yan T, Chien B, Wissa A, Tawfick S. A crawling robot driven by multi-stable origami. *Smart Materials and Structures*. 2017;**26**(9):094007
- [74] Zhang Z, Chen G, Wu H, Kong L, Wang H. A pneumatic/cable-driven hybrid linear actuator with combined structure of origami chambers and deployable mechanism. *IEEE Robotics and Automation Letters*. 2020;**5**(2):3564-3571
- [75] Bhovad P, Kaufmann J, Li S. Peristaltic locomotion without digital controllers: Exploiting multi-stability in origami to coordinate robotic motion. *Extreme Mechanics Letters*. 2019;**32**:100552
- [76] Nishikawa J. Kresling Origami-Based, Magnetically Actuated Crawling Robot for Drug Delivery. The Ohio State University; 2021
- [77] Mendoza MJ, Gollob SD, Lavado D, Koo BHB, Cruz S, Roche ET, et al. A vacuum-powered artificial muscle designed for infant rehabilitation. *Micromachines*. 2021;**12**(8):971
- [78] Kulasekera AL, Arumathanthri RB, Chathuranga DS, Gopura R, Lalitharatne TD. A thin-walled vacuum actuator (ThinVAc) and the development of multi-filament actuators for soft robotic applications. *Sensors and Actuators A: Physical*. 2021;**332**:113088
- [79] Oguntosin V, Akindele A. Design and characterization of artificial muscles from wedge-like pneumatic soft modules. *Sensors and Actuators A: Physical*. 2019;**297**:111523
- [80] Kulasekera AL, Arumathanthri RB, Chathuranga DS, Gopura R, Lalitharatne TD. A Low-Profile Vacuum Actuator (LPVAc) with integrated inductive displacement sensing for a novel sit-to-stand assist exosuit. *IEEE Access*. 2021;**9**:117067-117079
- [81] Weerasooriya LS, Chathuranga B, Somaratna OI, Kulasekera AL, Arumathanthri RB, Chathuranga DS, A novel contractile vacuum actuator and multi-actuator development for knee extension assist. 2021 IEEE 4th International Conference on Soft Robotics (RoboSoft); 2021
- [82] Kulasekera AL, Arumathanthri RB, Chathuranga DS, Lalitharatne TD, Gopura RC, A low-profile vacuum actuator: Towards a sit-to-stand assist exosuit. 2020 3rd IEEE International

Conference on Soft Robotics (RoboSoft); 2020

[83] Bruzek R, Biess L, Al-Nazer L, Development of rail temperature predictions to minimize risk of track buckle derailments. ASME/IEEE Joint Rail Conference; 2013

[84] Singamaneni S, Tsukruk VV. Buckling instabilities in periodic composite polymeric materials. *Soft Matter*. 2010;6(22):5681-5692

[85] Chen D, Yoon J, Chandra D, Crosby AJ, Hayward RC. Stimuli-responsive buckling mechanics of polymer films. *Journal of Polymer Science Part B: Polymer Physics*. 2014; 52(22):1441-1461

[86] Hu N, Burgueño R. Buckling-induced smart applications: Recent advances and trends. *Smart Materials and Structures*. 2015;24(6):063001

[87] Rogers JA, Someya T, Huang Y. Materials and mechanics for stretchable electronics. *Science*. 2010;327(5973): 1603-1607

[88] Wang Y, Yang R, Shi Z, Zhang L, Shi D, Wang E, et al. Super-elastic graphene ripples for flexible strain sensors. *ACS Nano*. 2011;5(5):3645-3650

[89] Shim J, Perdigou C, Chen ER, Bertoldi K, Reis PM. Buckling-induced encapsulation of structured elastic shells under pressure. *Proceedings of the National Academy of Sciences*. 2012; 109(16):5978-5983

[90] Florijn B, Coulais C, van Hecke M. Programmable mechanical metamaterials. *Physical Review Letters*. 2014;113(17):175503

[91] Wang P, Casadei F, Shan S, Weaver JC, Bertoldi K. Harnessing

buckling to design tunable locally resonant acoustic metamaterials. *Physical Review Letters*. 2014;113(1): 014301

[92] Yang D, Verma MS, So JH, Mosadegh B, Keplinger C, Lee B, et al. Buckling pneumatic linear actuators inspired by muscle. *Advanced Materials Technologies*. 2016;1(3):1600055

[93] Overvelde JT, Kloek T, D'haen JJ, Bertoldi K. Amplifying the response of soft actuators by harnessing snap-through instabilities. *Proceedings of the National Academy of Sciences*. 2015; 112(35):10863-10868

[94] Robertson MA, Paik J. New soft robots really suck: Vacuum-powered systems empower diverse capabilities. *Science Robotics*. 2017;2(9):eaan6357

[95] Hwang Y, Paydar OH, Candler RN. Pneumatic microfinger with balloon fins for linear motion using 3D printed molds. *Sensors and Actuators A: Physical*. 2015;234:65-71

[96] Mosadegh B, Polygerinos P, Keplinger C, Wennstedt S, Shepherd RF, Gupta U, et al. Pneumatic networks for soft robotics that actuate rapidly. *Advanced Functional Materials*. 2014; 24(15):2163-2170

[97] Onal CD, Rus D, A modular approach to soft robots. 2012 4th IEEE RAS & EMBS International Conference on Biomedical Robotics and Biomechatronics (BioRob); 2012

[98] TolleyMichael T, ShepherdRobert F, GallowayKevin C, WoodRobert J, WhitesidesGeorge M. A resilient, untethered soft robot. *Soft Robotics*. 2014;1(3)

[99] Balak R, Mazumdar YC, Multi-modal pneumatic actuator for twisting,

extension, and bending. 2020 IEEE/RSJ International Conference on Intelligent Robots and Systems (IROS); 2020

[100] Ge L, Dong L, Wang D, Ge Q, Gu G. A digital light processing 3D printer for fast and high-precision fabrication of soft pneumatic actuators. *Sensors and Actuators A: Physical*. 2018; **273**:285-292

[101] Wang X, Zhou H, Kang H, Au W, Chen C. Bio-inspired soft bistable actuator with dual actuations. *Smart Materials and Structures*. 2021; **30**(12): 125001

[102] Yap HK, Ng HY, Yeow C-H. High-force soft printable pneumatics for soft robotic applications. *Soft Robotics*. 2016; **3**(3):144-158

[103] Zhang YF, Zhang N, Hingorani H, Ding N, Wang D, Yuan C, et al. Fast-response, stiffness-tunable soft actuator by hybrid multimaterial 3D printing. *Advanced Functional Materials*. 2019; **29**(15):1806698

[104] Peele BN, Wallin TJ, Zhao H, Shepherd RF. 3D printing antagonistic systems of artificial muscle using projection stereolithography. *Bioinspiration & Biomimetics*. 2015; **10**(5):055003

[105] Mutlu R, Tawk C, Alici G, Sariyildiz E. A 3D printed monolithic soft gripper with adjustable stiffness. *IECON 2017-43rd Annual Conference of the IEEE Industrial Electronics Society*; 2017

[106] Tawk C, in het Panhuis M, Spinks GM, Alici G. Bioinspired 3D printable soft vacuum actuators for locomotion robots, grippers and artificial muscles. *Soft Robotics*. 2018; **5**(6):685-694

[107] Stano G, Percoco G. Additive manufacturing aimed to soft robots

fabrication: A review. *Extreme Mechanics Letters*. 2021; **42**:101079

[108] Rahim TNAT, Abdullah AM, Md A. Recent developments in fused deposition modeling-based 3D printing of polymers and their composites. *Polymer Reviews*. 2019; **59**(4):589-624

[109] Kamran M, Saxena A. A comprehensive study on 3D printing technology. *MIT International Journal of Mechanical Engineering*. 2016; **6**(2):63-69

[110] Lewis JA. Direct ink writing of 3D functional materials. *Advanced Functional Materials*. 2006; **16**(17): 2193-2204

[111] Khosravani MR, Reinicke T. On the environmental impacts of 3D printing technology. *Applied Materials Today*. 2020; **20**:100689

[112] Tee YL, Peng C, Pille P, Leary M, Tran P. PolyJet 3D printing of composite materials: Experimental and modelling approach. *Jom*. 2020; **72**(3):1105-1117

[113] Byrne O, Coulter F, Glynn M, Jones JF, Ní Annaidh A, O'Cearbhaill ED, et al. Additive manufacture of composite soft pneumatic actuators. *Soft Robotics*. 2018; **5**(6):726-736

[114] Stano G, Arleo L, Percoco G. Additive manufacturing for soft robotics: Design and fabrication of airtight, monolithic bending PneuNets with embedded air connectors. *Micromachines*. 2020; **11**(5):485

[115] Qi S, Guo H, Fu J, Xie Y, Zhu M, Yu M. 3D printed shape-programmable magneto-active soft matter for biomimetic applications. *Composites Science and Technology*. 2020; **188**:107973

[116] Al-Rubaiai M, Pinto T, Qian C, Tan X. Soft actuators with stiffness and

- shape modulation using 3D-printed conductive polylactic acid material. *Soft Robotics*. 2019;**6**(3):318-332
- [117] Robertson MA, Paik J, Low-inertia vacuum-powered soft pneumatic actuator coil characterization and design methodology. 2018 IEEE International Conference on Soft Robotics (RoboSoft); 2018
- [118] Rus D, Tolley MT. Design, fabrication and control of soft robots. *Nature*. 2015;**521**(7553):467-475
- [119] Sachyani Keneth E, Kamyshny A, Totaro M, Beccai L, Magdassi S. 3D printing materials for soft robotics. *Advanced Materials*. 2021;**33**(19):2003387
- [120] Zhou W, Li Y. Modeling and analysis of soft pneumatic actuator with symmetrical chambers used for bionic robotic fish. *Soft Robotics*. 2020;**7**(2):168-178
- [121] Moseley P, Florez JM, Sonar HA, Agarwal G, Curtin W, Paik J. Modeling, design, and development of soft pneumatic actuators with finite element method. *Advanced Engineering Materials*. 2016;**18**(6):978-988
- [122] Joe S, Totaro M, Beccai L. Analysis of soft Kirigami unit cells for tunable stiffness architectures. In: 2021 IEEE 4th International Conference on Soft Robotics (RoboSoft). 2021
- [123] Park S, Mondal K, Treadway RM III, Kumar V, Ma S, Holbery JD, et al. Silicones for stretchable and durable soft devices: Beyond Sylgard-184. *ACS Applied Materials & Interfaces*. 2018;**10**(13):11261-11268
- [124] Moučka R, Sedláčik M, Osička J, Pata V. Mechanical properties of bulk Sylgard 184 and its extension with silicone oil. *Scientific Reports*. 2021;**11**(1):1-9
- [125] Calderón AA, Ugalde JC, Zagal JC, Pérez-Arancibia NO. Design, fabrication and control of a multi-material-multi-actuator soft robot inspired by burrowing worms. In: 2016 IEEE international conference on robotics and biomimetics (ROBIO). 2016
- [126] Ding L, Dai N, Mu X, Xie S, Fan X, Li D, et al. Design of soft multi-material pneumatic actuators based on principal strain field. *Materials & Design*. 2019;**182**:108000
- [127] Fu H-C, Ho JD, Lee K-H, Hu YC, Au SK, Cho K-J, et al. Interfacing soft and hard: A spring reinforced actuator. *Soft Robotics*. 2020;**7**(1):44-58
- [128] L-y Z, Gao Q, J-z F, Q-y C, Zhu J-p, Sun Y, et al. Multimaterial 3D printing of highly stretchable silicone elastomers. *ACS Applied Materials & Interfaces*. 2019;**11**(26):23573-23583
- [129] Totaro M, Bernardeschi I, Wang H, Beccai L. Analysis and optimization of fully foam-based capacitive sensors. In: 2020 3rd IEEE International Conference on Soft Robotics (RoboSoft). 2020
- [130] Joe S, Wang H, Totaro M, Beccai L. Sensing deformation in vacuum driven foam-based actuator via inductive method. *Front Robot AI*. 2021;**8**:742885
- [131] Wang H, Bernardeschi I, Beccai L. Developing reliable foam sensors with novel electrodes. In: 2019 IEEE Sensors. 2019
- [132] Nakayama R, Suzuki R, Nakamaru S, Niiyama R, Kawahara Y, Kakehi Y. MorphIO: Entirely soft sensing and actuation modules for programming shape changes through tangible interaction. In: Proceedings of the 2019

on Designing Interactive Systems
Conference. 2019

[133] Wang H, Totaro M, Beccai L.
Toward perceptive soft robots: Progress
and challenges. *Advanced Science*. 2018;
5(9):1800541

[134] Jiang Y, Wang Q. Highly-
stretchable 3D-architected mechanical
metamaterials. *Scientific Reports*. 2016;
6(1):1-11

[135] Janbaz S, Bobbert F, Mirzaali M,
Zadpoor A. Ultra-programmable
buckling-driven soft cellular
mechanisms. *Materials Horizons*. 2019;
6(6):1138-1147

[136] Kaur M, Kim WS. Toward a smart
compliant robotic gripper equipped with
3D-designed cellular fingers. *Advanced
Intelligent Systems*. 2019;1(3):1900019

[137] Ge Q, Chen Z, Cheng J, Zhang B,
Zhang Y-F, Li H, et al. 3D printing of
highly stretchable hydrogel with diverse
UV curable polymers. *Science advances*.
2021;7(2):eaba4261

[138] PROBOSCIdean Sensitive Soft
Robot for Versatile Gripping. 2019.
H2020-FETOPEN, Grant n. 863212.
2022. Available from: <https://proboscis.eu/> [Accessed: January 24, 2022].